PHYSICAL REVIEW B **84**, 174511 (2011)

Eliashberg approach to infrared anomalies induced by the superconducting state of $Ba_{0.68}K_{0.32}Fe_2As_2$ single crystals

A. Charnukha,[1] O. V. Dolgov,[1] A. A. Golubov,[2] Y. Matiks,[1] D. L. Sun,[1] C. T. Lin,[1] B. Keimer,[1] and A. V. Boris[1]

[1]*Max-Planck-Institut für Festkörperforschung, Heisenbergstrasse 1, D-70569 Stuttgart, Germany*

[2]*Faculty of Science and Technology and MESA+ Institute of Nanotechnology, NL-7500 AE Enschede, The Netherlands*

(Received 4 March 2011; revised manuscript received 1 November 2011; published 18 November 2011)

We report the full complex dielectric function of high-purity $Ba_{0.68}K_{0.32}Fe_2As_2$ single crystals with $T_c = 38.5$ K determined by wideband spectroscopic ellipsometry at temperatures $10 \leqslant T \leqslant 300$ K. We discuss the microscopic origin of superconductivity-induced infrared optical anomalies in the framework of a multiband Eliashberg theory with two distinct superconducting gap energies, $2\Delta_A \approx 6\ k_B T_c$ and $2\Delta_B \approx 2.2\ k_B T_c$. The observed unusual suppression of the optical conductivity in the superconducting state at energies up to $14\ k_B T_c$ can be ascribed to spin-fluctuation–assisted processes in the clean limit of the strong-coupling regime.

DOI: 10.1103/PhysRevB.84.174511 PACS number(s): 74.25.Gz, 74.20.Mn, 74.70.Xa, 78.30.−j

I. INTRODUCTION

The discovery of iron-based superconductors[1] has generated significant experimental and theoretical effort to unravel the mechanism of high-temperature superconductivity in these compounds. This effort has yielded a comprehensive experimental description of the electronic structure at the Fermi level, which includes multiple Fermi surface sheets in good agreement with density functional calculations.[2,3] Partial nesting between at least two of these sheets leads to a spin-density-wave instability that renders the metallic parent compounds antiferromagnetic. In the superconducting compounds, spin fluctuations become the source of strong repulsive interband interactions and might give rise to superconductivity with different signs on these sheets.[4]

The most incisive experimental data have been obtained on high-quality single crystals of iron pnictides with the so-called 122 structure, for instance, $BaFe_2As_2$, with K substituted for Ba or Co for Fe, resulting in hole and electron doping, respectively. In all of these materials, five Fermi surface sheets have been identified in calculations and confirmed by numerous independent experimental studies:[2,3] in the reduced Brillouin-zone scheme, these are three hole pockets at the Γ point and two almost degenerate electron pockets at the X point with nesting between the hole and electron sheets. Among all of these 122 materials, the optimally hole-doped compound $Ba_{0.68}K_{0.32}Fe_2As_2$ (BKFA) has the highest transition temperature of 38.5 K. Due to their exceptional quality, crystals of this compound are well suited as a test bed for theoretical models. A four-band Eliashberg theory with strong interband coupling has already proven successful in accounting for the transition temperature, as well as the temperature dependence of the free energy and superconducting gaps of this compound.[5] This analysis has made clear that a satisfactory description of the bulk thermodynamical properties in the superconducting state can only be obtained via strong coupling to spin fluctuations or other bosons with spectral weight below 50 meV.

In this work, we extend the approach of Ref. 5 to describe the far-infrared properties of the same BKFA single crystal. We show that major characteristic features of superconductivity can be explained within a strong-coupling Eliashberg approach with two distinct values of the superconducting energy gap, $2\Delta_A \approx 6\ k_B T_c$ and $2\Delta_B \approx 2.2\ k_B T_c$, in quantitative agreement with angle-resolved photoemission,[6–9] scanning tunneling microscopy,[10,11] and specific-heat measurements.[5] We also demonstrate that within this approach, the difference in the shape of the infrared conductivity spectra of hole- and electron-doped 122 compounds is reproduced by strong-coupling calculations in the clean and dirty limits (weak and strong impurity scattering), respectively.

II. EXPERIMENTAL DETAILS

The optimally doped BKFA single crystals were grown in zirconia crucibles sealed in quartz ampoules under argon atmosphere.[12] From dc resistivity, magnetization, and specific-heat measurements, we obtained $T_c = 38.5 \pm 0.2$ K. The sample surface was cleaved prior to every optical measurement. The full complex dielectric function $\varepsilon(\omega)$ was obtained in the range 0.01–6.5 eV using broadband ellipsometry, as described in Ref. 13. In this work, we focus on the itinerant charge-carrier response contained within the far-infrared spectral range measured at the infrared beam line of the ANKA synchrotron light source at the Karlsruhe Institute of Technology, Germany.

III. RESULTS AND DISCUSSION

A. Far-infrared conductivity

The optical response of BKFA in the far-infrared spectral range is shown in Figs. 1(a) and 1(b), respectively, for the real parts of optical conductivity $\sigma(\omega) = \sigma_1(\omega) + i\sigma_2(\omega)$ and dielectric function $\varepsilon(\omega) = 1 + 4\pi i\sigma(\omega)/\omega$. It is dominated by the contribution of the itinerant charge carriers manifested in negative values of $\varepsilon_1(\omega)$. Figure 1(a) also reveals a peak around 15–20 meV in $\sigma_1(\omega)$ with a concomitant upturn in $\varepsilon_1(\omega)$ at higher temperatures, indicating the presence of a collective excitation. The superconducting transition is accompanied by a suppression of the optical conductivity up to 50 meV ($14\ k_B T_c$). The corresponding missing area in $\sigma_1(\omega)$ between 41 and 10 K, $\int_{0^+}^{6\Delta_A} \Delta\sigma_1(\omega)d\omega = (8\lambda_L^2)^{-1}$, manifests itself as a characteristic $-1/(\lambda_L\omega)^2$ contribution to $\varepsilon_1(\omega)$ in Fig. 1(b) in the superconducting state. The low-temperature London penetration depth $\lambda_L(10\text{ K}) = 2200$ Å extracted from these data is consistent with other measurements.[14] Application of a Kramers-Kronig consistency check (as described in the

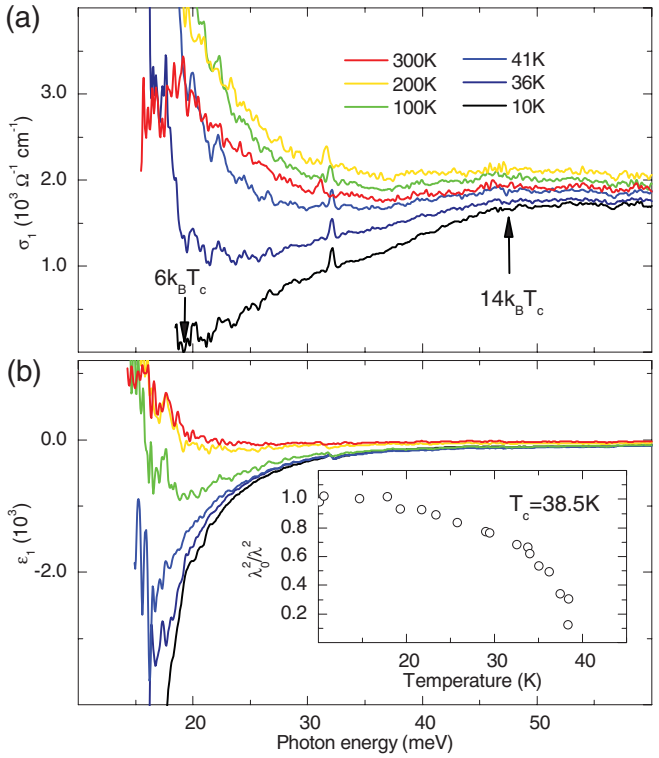

FIG. 1. (Color online) Real part of the (a) optical conductivity and (b) dielectric function in the far-infrared spectral region. Two characteristic superconductivity energy scales are present: 6 and 14 k_BT_c. Inset: Temperature dependence of the normalized inverse penetration depth obtained via a Kramers-Kronig consistency procedure.

supplementary material to Ref. 15) to determine the spectral weight contained in the extrapolation region below 10 meV allows one to rather accurately determine the temperature dependence of the London penetration depth. The resulting profile is shown in the inset in Fig. 1 for $1/\lambda_L(T)^2$ normalized to its value at 10 K.

At energies close to the optical superconducting gap $2\Delta_A \approx$ 20 meV, one of the directly measured ellipsometric angles $\Psi(\omega)$ approaches its critical value of 45° at the superconducting transition, which implies that the reflectivity of the sample approaches unity and its optical conductivity $\sigma_1(\omega)$ is close to zero. Remarkably, Fig. 1(a) shows a quasilinear dependence of $\sigma_1(\omega)$ in the superconducting state from $2\Delta_A$ to as high as 14 k_BT_c, in stark contrast to the electron-doped 122 compounds.[16–18] In the latter, the optical conductivity at $2\Delta_A$ decreases abruptly upon cooling below T_c, but only a weak superconductivity-induced modification is observed at higher energies. The quasilinear behavior in BKFA cannot be reconciled with the Mattis-Bardeen theory,[19] which is widely used for pnictides and is a weak-coupling extension of the BCS theory to finite impurity scattering. As all optimally-doped 122 pnictide superconductors appear to be in the strong-coupling regime, the Eliashberg theory[20] has to be used in order to obtain an adequate description of the optical properties.

B. Interband optical transitions

The analysis of the free-charge-carrier response implies that the contribution of all interband transitions needs to be eliminated from the experimentally obtained optical conductivity. The total spectral weight of these transitions gives rise to a nonvanishing contribution $\Delta\varepsilon_{tot}$ to the real part of the far-infrared dielectric function $\varepsilon_1(\omega)$. In iron pnictides, $\Delta\varepsilon_{tot}$ has a particularly large value due to the high polarizability of the Fe-As bonds.[15]

TABLE I. Parameters of the Lorentzian terms in Eq. (1) obtained from the analysis of the interband transitions in the optimally doped BKFA; separate terms are shown in Fig. 2 as solid black lines.

j	$\Delta\varepsilon_j$	ω_{0j} (cm^{-1})	Γ_j (cm^{-1})
1	44.37	4784.4	10243.0
2	5.67	6703.3	8557.4
3	1.10	13977.1	8914.0
4	7.31	20848.9	30158.4
5	0.473	23182.8	10268.9
6	2.54	58812.7	38689.8

The full complex dielectric function $\varepsilon(\omega) = \varepsilon_1(\omega) + i\varepsilon_2(\omega)$ of $Ba_{0.68}K_{0.32}Fe_2As_2$, obtained experimentally in the range from 12 meV to 6.7 eV, was analyzed using

$$\varepsilon^{\text{inter}}(\omega) = \varepsilon_\infty + \sum_{j=1}^{n} \frac{\Delta\varepsilon_j \omega_{0j}^2}{\left(\omega_{0j}^2 - \omega^2\right) - i\Gamma_j\omega}, \qquad (1)$$

where ε_∞ is the core contribution to the dielectric function, and $\Delta\varepsilon_j$, ω_{0j}, and Γ_j are the static permittivity contribution, center frequency, and width of the Lorentzian oscillators used to model the interband transitions, respectively. These parameters were obtained by a simultaneous fit of both the real and imaginary parts of the dielectric function and are listed in Table I. The remaining free-charge-carrier response will be analyzed in the following sections.

The results of such an analysis are presented in Fig. 2 for $Ba_{0.68}K_{0.32}Fe_2As_2$ at 10 K (where the blue line is the experimental data, and the black lines are the separate Lorentz contributions). To display the scale of the temperature-induced variation of the interband transitions, the experimental spectrum at 300 K is also shown (red, far-left line). The lowest interband transition in this material lies around 0.5 eV and significantly contributes to the optical polarizability of the system, as will be discussed in the next section. An unscreened bare plasma frequency of 1.6 eV at 41 K was consistently obtained from the spectral weight of the itinerant response, $SW_{it} = \int_0^\infty \sigma_1^{it}(\omega)d\omega$, as $\omega_{pl} = \sqrt{8SW_{it}}$ and a simultaneous fit of the real and imaginary parts of the dielectric function at high energies.

C. Extended Drude model

Signatures of a boson pairing mediator of the Eliashberg theory come from a qualitative analysis of the optical conductivity within the extended Drude model. It implies that the optical scattering rate is related to the far-infrared optical response as $\gamma(\omega) = \text{Re}[\omega_{pl}^2/4\pi\sigma^{it}(\omega)]$, where ω_{pl} is the plasma frequency of the free charge carriers. The superscript "it" stands for "itinerant" and implies that the contribution of all interband transitions has been subtracted from the experimentally obtained optical conductivity, as described in the previous section. The optical scattering rate shows clear evidence of an

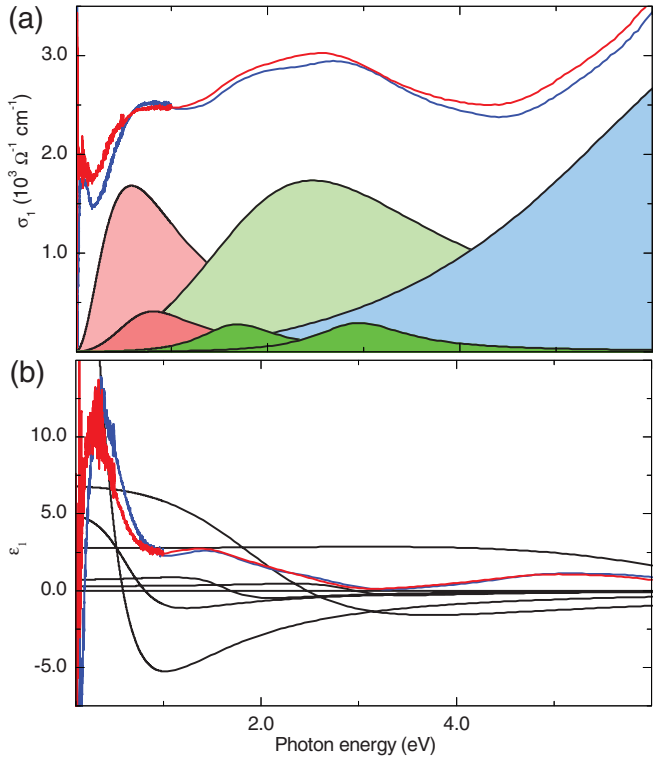

FIG. 2. (Color online) Real part of the (a) optical conductivity and (b) dielectric function of $Ba_{0.68}K_{0.32}Fe_2As_2$ at 300 K (red line, far left) and 10 K (blue line). Interband transitions inferred from the dispersion analysis (solid black lines).

intermediate boson irrespective of complications due to the multiband character of the compound. Figure 3 plots $\gamma(\omega)$ of BKFA at 41 K [blue (dark gray) line] and 10 K (black line) for $\omega_{\rm pl} = 1.6$ eV, with all interband transitions subtracted in both cases [the itinerant spectral weight $SW_{\rm it}$ corresponds to the blue (upper) shaded area in Fig. 4(a)]. In the superconducting state, no scattering is expected up to photon energies exceeding the binding energy of the Cooper pairs. Thus, the onset of the

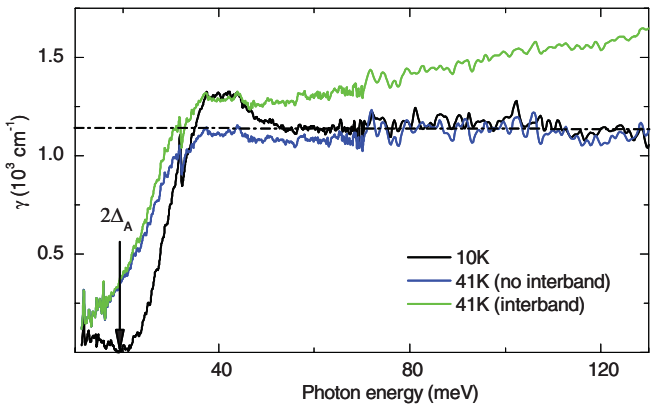

FIG. 3. (Color online) Optical scattering rate obtained from the experimental data at 41 and 10 K within the extended Drude model, with the contribution of the interband transitions subtracted [blue (dark gray) and black lines, respectively] and at 41 K without subtraction [green (light gray) line]. Dash-dotted line indicates the saturation level of the high-energy optical scattering rate.

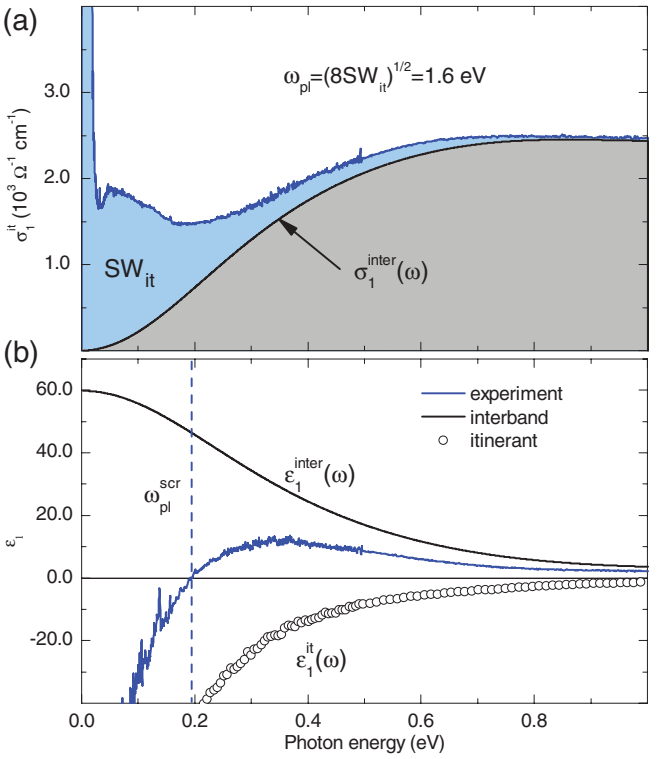

FIG. 4. (Color online) (a) Real part of the optical conductivity at 41 K [blue (gray) line]. The contribution of itinerant charge carriers [blue (upper) area] is obtained by subtracting all interband transitions $\sigma_1^{\rm inter}(\omega)$ [gray (lower) area] from the optical response. (b) Real part of the dielectric function at 41 K [blue (gray) line]. The free-charge-carrier response $\varepsilon_1^{\rm it}(\omega)$ (open circles) is obtained by eliminating all interband transitions $\varepsilon_1^{\rm inter}(\omega)$ (black solid line). The blue dashed line indicates the screened plasma frequency at 41 K.

optical scattering rate in Fig. 3 marks the optical energy gap $2\Delta_{\rm A} \approx 20$ meV. Saturation of $\gamma(\omega > 50\ {\rm meV})$ at 1100 $\rm cm^{-1}$ indicates that the boson spectral function is contained well below 50 meV.[21] It is important to emphasize that due to the multiband character of the iron pnictides, an analysis of the optical scattering rate in the framework of a single-band Eliashberg theory is potentially misleading. Moreover, also shown in Fig. 3 is a spectrum that directly results from the experimental data, without accounting for the interband transitions. It becomes clear that an increase in the scattering rate at higher energies that might be ascribed to strong electron correlations can result from an unsubtracted contribution of the interband transitions to the complex optical conductivity. This is especially important in iron pnictides, since the lowest-lying interband transition at about 0.5 eV contributes to an anomalously large value of the low-energy dielectric permittivity, $\Delta\varepsilon_{\rm tot} = \sum_{j=1}^{n} \Delta\varepsilon_j \approx 60$ (see Table I). This value is clearly seen in Fig. 4(b) as the zero-frequency limit of $\varepsilon_1^{\rm inter}(\omega)$ determined by means of the dispersion analysis. It is also fully consistent with the bare plasma frequency of 1.6 eV and the zero crossing in $\varepsilon_1(\omega)$ at 0.2 eV [blue (gray) line in Fig. 4(b)]. Such $\Delta\varepsilon_{\rm tot}$ is thus an order of magnitude larger than in any other high-temperature superconductor (e.g., ≈5 in cuprates).[22] Recently, a similarly high value in a conventional

superconductor was inferred from reflectivity measurements on elemental bismuth.[23]

IV. EFFECTIVE TWO-BAND MODEL FOR IRON PNICTIDES

A. Four-band Eliashberg theory

To determine the microscopic origin of the high-energy anomaly $2\Delta_A < \hbar\omega < 14\ k_B T_c$ in the real part of the optical conductivity in Fig. 1(a), we use a four-band Eliashberg theory[20,24,25] that proved successful in explaining thermodynamic data obtained on the same compound.[5]

The main ingredient of the theory is the total spectral function of the electron-boson interaction $B(\omega)$ [Eliashberg function; analogous to that of the electron-phonon interaction $\alpha^2 F(\omega)$]. In a four-band system, it can be decomposed into 16 functions, $B(\omega)_{ij}$, where i and j label the four Fermi surface sheets ($i, j = 1,2,3,4$). The *standard* Eliashberg functions determine the superconducting and thermodynamic properties, such as the superconducting transition temperature and gaps, electronic specific heat, de Haas-van Alphen mass renormalizations, etc., and are defined as

$$B(\omega)_{ij} = \frac{1}{N_i} \sum_{\mathbf{k},\mathbf{k}',\nu} \left|g^{ij,\nu}_{\mathbf{k},\mathbf{k}'}\right|^2 \delta\left(\varepsilon^i_{\mathbf{k}}\right)\delta\left(\varepsilon^j_{\mathbf{k}'}\right)\delta\left(\omega - \omega^{\nu}_{\mathbf{k}-\mathbf{k}'}\right),$$

where N_i is the partial density of states per spin on the ith sheet of the Fermi surface, and $g^{ij}_{\mathbf{k},\mathbf{k}'}$ is the matrix element of electron-boson interactions.

The transport and electrodynamical properties are defined by 16 *transport* Eliashberg functions (which enter the Boltzmann kinetic equation),

$$B(\omega)^{\alpha\beta}_{\mathrm{tr},ij} = \frac{1}{2N_i\left\langle v^{\alpha\ 2}_{\mathrm{F},i}\right\rangle} \sum_{\mathbf{k},\mathbf{k}',\nu} \left|g^{ij\nu}_{\mathbf{k}\mathbf{k}'}\right|^2 \times \left[v^{\alpha}_{\mathrm{F},i}(\mathbf{k}) - v^{\beta}_{\mathrm{F},j}(\mathbf{k}')\right]^2 \delta\left(\varepsilon^i_{\mathbf{k}}\right)\delta\left(\varepsilon^j_{\mathbf{k}'}\right)\delta\left(\omega - \omega^{\nu}_{\mathbf{k}-\mathbf{k}'}\right),$$

where $v^{\alpha}_{\mathrm{F},i}$ is the αth Cartesian component of the Fermi velocity on Fermi surface i. The average Fermi velocity is related to the plasma frequency by the standard expression $\omega^2_{\mathrm{pl},i} = 8\pi e^2 N_i \langle v^2_{\mathrm{F},i}\rangle = 8\pi e^2 \sum_{\mathbf{k}} v^2_{\mathrm{F},i}(\mathbf{k})\delta(\varepsilon^i_{\mathbf{k}})$. All Eliashberg functions satisfy the symmetry relations $M_i B_{ij} = M_j B_{ji}$, where $M_i = N_i$ and $M_i = \omega^2_{\mathrm{pl},i}$ for the standard and transport Eliashberg functions, respectively.

As a starting point, we consider a four-band model based on the band-structure calculations with two hole bands and two electron bands crossing the Fermi level that has proven successful in accounting for the thermodynamic properties of BKFA.[5] We use the same input parameters, namely, the densities of states $N_1 = 22$, $N_2 = 25$, and $N_3 = N_4 = 7$ states per Rydberg and per unit cell, with the first two having a hole and the other two having an electron character. The main input, the spectral function of the intermediate boson, was taken the same as in Fig. S4 of Ref. 5 in the form of a spin-fluctuation spectrum $\tilde{B}_{ij}(\Omega) = \lambda_{ij} f(\Omega/\Omega_{sf})$ with a linear ω dependence at low frequencies. Here, λ_{ij} is the coupling-constant pairing band i with band j and Ω_{SF} is a characteristic spin-fluctuation frequency, the values of which correspond to those in Table SII of Ref. 5: $\Omega_{sf} = 13$ meV and

$$\lambda_{ij} = \begin{pmatrix} 0.2 & 0 & -1.7 & -1.7 \\ 0 & 0.2 & -0.25 & -0.25 \\ -5.34 & -0.89 & 0.2 & 0 \\ -5.34 & -0.89 & 0 & 0.2 \end{pmatrix}. \quad (2)$$

Negative elements correspond to *interband* hole-electron repulsion, while the positive elements correspond to *intraband* attraction.

The 4×4 matrix of coupling constants and four densities of states characterizing this model are highly constrained by thermodynamic, transport, and photoemission data,[5–8,10,11] and the same set of parameters is used here. In principle, an additional set of four plasma frequencies and a 4×4 matrix of intraband-interband impurity scattering rates has to be taken into account to describe the optical response. However, this parameter set can be strongly reduced based on the following considerations.

B. Role of impurities and defects

Both normal and superconducting properties of a multiband superconductor significantly depend on impurity scattering. Unlike in conventional superconductivity, one has to distinguish between the intraband impurity scattering, which does not add any new physics (in the Born approximation) compared with single-band superconductivity, and *interband* scattering, which in many cases has an effect comparable to the pair-breaking effect of magnetic impurities (or of nonmagnetic impurities in superconductors with p- or d-wave pairing).[26] In this regard, the fact that no strong correlation has been observed between the residual resistivity (which indirectly characterizes the impurity scattering) and the critical temperature T_c of the (nearly) optimally electron-doped BKFA (see Table II) indicates that the level of *interband* impurities in the Born limit is very small. Thus, one only needs to estimate the intraband scattering rates.

C. Reduction to a two-band model

A substantial simplification can further be made by a projection of the four-band model onto an effective two-band model, motivated by the observation of two distinct groups of superconducting energy gaps in a variety of experiments.[5–8,10,11] These gaps can be identified as a single gap Δ_B on the outer holelike Fermi surface and a group of three gaps of magnitude $\sim\Delta_A$ on the inner holelike and two electronlike Fermi surfaces.

TABLE II. Superconducting transition temperature and residual resistivity $\rho_{40\,\mathrm{K}}$ of (nearly) optimally hole-doped BKFA.

T_c (K)	Residual resistivity (mΩ cm)	Reference
38.5	0.04	5
38	0.075	27
38	0.1	28
36.5	0.055	29

In general, the superconducting order parameters are a solution of a linear system of equations,

$$e_i = \sum_{j=1}^{4} B_{ij}(\omega) e_j. \tag{3}$$

The Eliashberg functions $B_{ij}(\omega)$ satisfy the symmetry relations

$$N_i B_{ij}(\omega) = N_j B_{ji}(\omega) \tag{4}$$

and, therefore, can be represented in the form $B_{ij}(\omega) = U_{ij}(\omega) N_j$, where U_{ij} is a symmetric matrix. Further, we can construct a functional

$$\mathfrak{F}\{e_i\} = \sum_{j=1}^{4} N_j e_j^2 - \sum_{i,j=1}^{4} N_i e_i U_{ij} N_j e_j. \tag{5}$$

Equation (3) then results from minimization of $\mathfrak{F}$ with respect to e_i. As mentioned above, BKFA has three gaps with very close absolute values (the first hole gap has the opposite sign with respect to the other two). Minimizing functional Eq. (5) subject to the additional constraints $e_3 = e_4 = -e_1 = \Delta_A$, and $e_2 = -\Delta_B$, one finds

$$\begin{pmatrix} \Delta_A \\ \Delta_B \end{pmatrix} = \begin{pmatrix} \lambda_{AA} & \lambda_{AB} \\ \lambda_{BA} & \lambda_{BB} \end{pmatrix} \begin{pmatrix} \Delta_A \\ \Delta_B \end{pmatrix}, \tag{6}$$

where the matrix elements satisfy

$$\lambda_{AA} = \frac{N_1(\lambda_{11} - 2\lambda_{13} - 2\lambda_{14}) + N_3\lambda_{33} + N_4\lambda_{44}}{N_1 + N_3 + N_4},$$
$$\lambda_{AB} = \frac{N_2(\lambda_{23} + \lambda_{24})}{N_1 + N_3 + N_4},$$
$$\lambda_{BA} = \lambda_{23} + \lambda_{24},$$
$$\lambda_{BB} = \lambda_{22}.$$

Given the boson spectrum centered at 13 meV (for details, see supplementary online material in Ref. 5) consistent with the energy of the spin-resonance excitation in this compound,[30,31] and assuming the matrix elements given by Eq. (2), one obtains the following two-band model coupling matrix:

$$\lambda_{IJ} = \begin{pmatrix} 4.36 & -0.35 \\ -0.5 & 0.2 \end{pmatrix}, \quad I, J = \{A, B\}. \tag{7}$$

The partial densities of states on the Fermi level of effective band A and band B are

$$N_A = N_1 + N_3 + N_4 = 36 \text{ states/(Rydberg u.c.)},$$
$$N_B = N_2 = 25 \text{ states/(Rydberg u.c.)}, \tag{8}$$

where "u.c." stands for "unit cell." The first effective intraband coupling constant is an order of magnitude larger than predicted for the intraband electron-phonon coupling.[32] It does not, however, have a direct physical meaning by itself, but rather incorporates contributions from *three* different bands. We reiterate that the coupling matrix has been inferred from prior measurements. This way only two intraband impurity scattering rates enter as free parameters of the theory in addition to the plasma frequencies of the bands.

The effective two-band model closely reproduces all the predictions of the four-band model, such as the superconducting transition temperature $T_c = 38.4$ K, superconducting gaps $\Delta_A = 9.7$ and $\Delta_B = 3.7$ meV, and free energy and superconducting gaps as functions of temperature, as shown in Figs. 5(a) and 5(b), respectively. The calculated densities of states N_A and N_B are very similar, in accordance with the partial Sommerfeld constants obtained in the treatment of the specific-heat data in a phenomenological two-band α model:[5] $\gamma_A \simeq \gamma_B$, where the Sommerfeld constant γ is related to the density of states per spin at the Fermi energy $N(0)$ via $\gamma = (1/3)\pi^2 k_B^2 N(0)$.

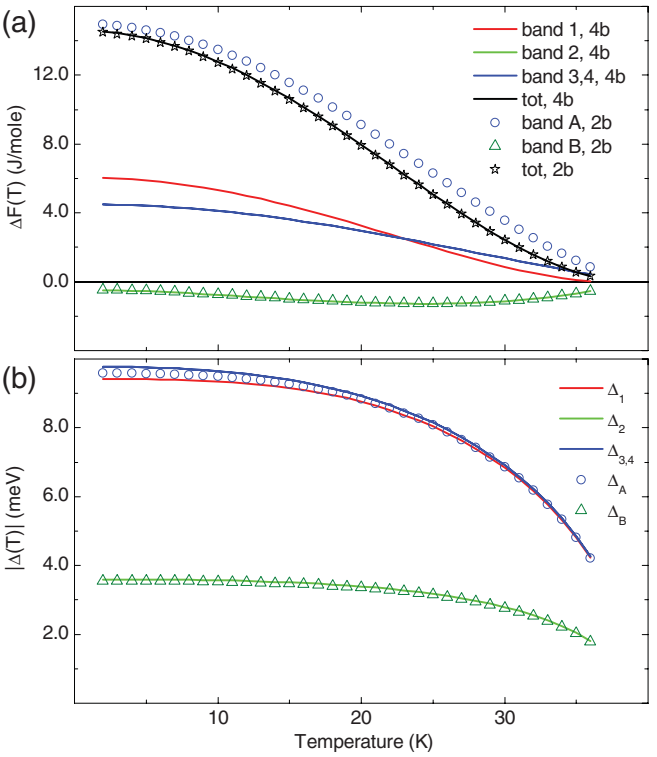

FIG. 5. (Color online) Temperature dependence of the (a) free energy and (b) superconducting gaps in the four-band (lines) and reduced two-band (symbol) models, with coupling matrices given by Eqs. (2) and (7), respectively.

D. Comparison with the experiment

In our calculation, we consider two clean bands with $\gamma_A = \gamma_B = 1$ cm^{-1}. As the bare plasma frequencies of all bands are similar, it follows that the spectral weight of band A has to be much larger than that of band B. Assigning 80% of the spectral weight to the effective band, we obtain the results presented as solid lines in Fig. 6(a). The high-energy anomaly at 14 $k_B T_c$ is naturally captured by the model without resorting to additional gaps.[33] This calculation also accounts for the fact that only the biggest superconducting gap is visible in the optical response of BKFA due to a small contribution of band B (20% of the spectral weight) to the overall optical conductivity. This leads to two possible levels of the impurity scattering rate of band B, which has to be either very small, $\gamma_B \approx 1$ cm^{-1}, or very large, at about 1000 cm^{-1}. The latter value provides a better description of the optical scattering rate (see Supplemental Material in Ref. 34 for interactive simulation). However, such a large disparity between the charge carriers is hard to reconcile with the Hall and de Haas-van Alphen experiments, which imply

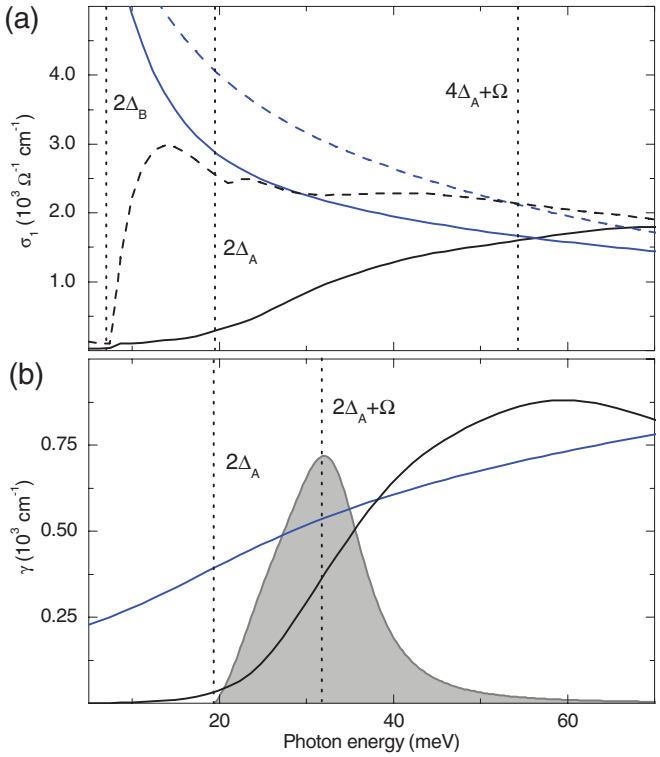

FIG. 6. (Color online) (a) Real part of the far-infrared conductivity obtained within the two-band Eliashberg theory (see text) at 40 K [blue (gray) lines] and 10 K (black lines) in the clean limit $\gamma_A = \gamma_B = 1$ cm^{-1} (solid lines) and dirty limit $\gamma_A = \gamma_B = 200$ cm^{-1} (dashed lines). (b) Optical scattering rate in the clean limit of the same model. The gray area shows the normalized boson spectral function $B(\omega)$ used in the calculation, displaced from zero by $2\Delta_A$ to assist interpretation in the superconducting state.[31]

that the impurity scattering rate of the holes is no more than one order of magnitude higher than that of the electrons.[35,36] This residual uncertainty notwithstanding, our results show that the impurity scattering rate of band A must be very small, because the energy $14k_BT_c \approx 4\Delta_A + \Omega$ is no longer discernible in the simulated spectra when γ_A increases (see Supplemental Material in Ref. 34 for an interactive simulation). Thus, the region of the linear increase of $\sigma_1(\omega)$ can only be observed in a very clean material.

The same reduced two-band model can be applied to the case of $BaFe_{1.85}Co_{0.15}As_2$ (BFCA). In this compound, the spin-resonance excitation occurs at a very similar energy of 10 meV.[37] A boson spectrum centered at this energy is also consistent with Andreev-reflection measurements.[38] Recently, a comprehensive specific-heat study of this compound at different Co-doping levels has been carried out.[39] The analysis of the experimental data in the framework of the two-band α model indicates that the largest gap develops in the band with the largest electronic density of states, providing further evidence that several bands contribute to the strongly coupled band in the reduced two-band model. Figure 6(a) (dashed lines) shows that a calculation within the same reduced two-band model qualitatively reproduces the far-infrared optical conductivity of BFCA[16–18] when both bands are assumed to be dirty with $\gamma_A = \gamma_B = 200$ cm^{-1} and a redistribution of the spectral weight between the bands is taken into account as $\omega^2_{pl,A} \approx \omega^2_{pl,B}$. The model captures the two prominent superconductivity-induced anomalies clearly observed in experiments: the steep onset of absorption at the value of the small gap $2\Delta_B$ and the weaker superconductivity-induced changes of the optical conductivity extending up to 18 k_BT_c. The redistribution of the spectral weight between the bands in BFCA compared to BKFA implied by our analysis is justified by doping with different carriers in the two compounds, while the large difference in their impurity scattering rates is a natural consequence of the difference in doping mechanisms by chemical substitution, which directly affects the FeAs layers in BFCA, but not in BKFA.

V. CONCLUSIONS

In summary, a qualitative description of superconductivity-induced optical anomalies in the far-infrared optical conductivity of $Ba_{0.68}K_{0.32}Fe_2As_2$ is obtained in the framework of an effective two-band Eliashberg theory with a strong coupling to spin fluctuations reduced from its four-band counterpart. The linear increase of absorption above the larger superconducting gap can only be observed when the effective band is extremely clean. The same model in the dirty limit gives a good qualitative explanation of the optical conductivity of the optimally electron-doped BFCA consistently in the strong-coupling regime. Our approach provides a universal description of the far-infrared conductivity of iron pnictides and clearly outlines the limitations of the Mattis-Bardeen theory, which has been widely used for analysis of essentially all Fe-based superconductors. Treatments beyond the Mattis-Bardeen theory are thus indispensable for the correct determination of the number and magnitudes of the superconducting gaps in clean materials.

ACKNOWLEDGMENTS

This project was supported by the German Science Foundation under Grant No. BO 3537/1-1 within SPP 1458. We gratefully acknowledge Y.-L. Mathis for support at the infrared beam line of the synchrotron facility ANKA at the Karlsruhe Institute of Technology, and P. Popovich for taking part in some of the measurements. A.A.G. acknowledges Dutch FOM for partial support.

[1] Y. Kamihara, T. Watanabe, M. Hirano, and H. Hosono, J. Am. Chem. Soc. **130**, 3296 (2008).
[2] J. Paglione and R. L. Greene, Nature Phys. **6**, 645 (2010).
[3] D. C. Johnston, Adv. Phys. **59**, 803 (2010).
[4] I. I. Mazin, Nature (London) **464**, 183 (2010).
[5] P. Popovich, A. V. Boris, O. V. Dolgov, A. A. Golubov, D. L. Sun, C. T. Lin, R. K. Kremer, and B. Keimer, Phys. Rev. Lett. **105**, 027003 (2010).

[6]D. V. Evtushinsky *et al*., Phys. Rev. B **79**, 054517 (2009).
[7]Y. Zhang *et al*., Phys. Rev. Lett. **105**, 117003 (2010).
[8]K. Nakayama, T. Sato, P. Richard, Y.-M. Xu, T. Kawahara, K. Umezawa, T. Qian, M. Neupane, G. F. Chen, H. Ding, and T. Takahashi, Phys. Rev. B **83**, 020501 (2011).
[9]Y.-M. Xu *et al*., Nature Phys. **7**, 198 (2011).
[10]L. Shan, Y. L. Wang, B. Shen, B. Zeng, Y. Huang, A. Li, D. Wang, H. Yang, C. Ren, Q. H. Wang, S. H. Pan, and H. H. Wen, Nature Phys. **7**, 325 (2011).
[11]L. Shan, Y.-L. Wang, J. Gong, B. Shen, Y. Huang, H. Yang, C. Ren, and H.-H. Wen, Phys. Rev. B **83**, 060510 (2011).
[12]G. L. Sun, D. L. Sun, M. Konuma, P. Popovich, A. Boris, J. B. Peng, K.-Y. Choi, P. Lemmens, and C. T. Lin, J. Supercond. Nov. Magn. **24**, 1773 (2011).
[13]A. V. Boris, N. N. Kovaleva, S. S. A. Seo, J. S. Kim, P. Popovich, Y. Matiks, R. K. Kremer, and B. Keimer, Phys. Rev. Lett. **102**, 027001 (2009).
[14]G. Li, W. Z. Hu, J. Dong, Z. Li, P. Zheng, G. F. Chen, J. L. Luo, and N. L. Wang, Phys. Rev. Lett. **101**, 107004 (2008).
[15]A. Charnukha, P. Popovich, Y. Matiks, D. L. Sun, C. T. Lin, A. N. Yaresko, B. Keimer, and A. V. Boris, Nature Commun. **2**, 219 (2011).
[16]J. J. Tu, J. Li, W. Liu, A. Punnoose, Y. Gong, Y. H. Ren, L. J. Li, G. H. Cao, Z. A. Xu, and C. C. Homes, Phys. Rev. B **82**, 174509 (2010).
[17]K. W. Kim, M. Rössle, A. Dubroka, V. K. Malik, T. Wolf, and C. Bernhard, Phys. Rev. B **81**, 214508 (2010).
[18]R. P. S. M. Lobo, Y. M. Dai, U. Nagel, T. Room, J. P. Carbotte, T. Timusk, A. Forget, and D. Colson, Phys. Rev. B **82**, 100506 (2010).
[19]W. Zimmermann, E. Brandt, M. Bauer, E. Seider, and L. Genzel, Phys. C **183**, 99 (1991).
[20]S. B. Nam, Phys. Rev. **156**, 470 (1967).
[21]S. Shulga, O. Dolgov, and E. Maksimov, Physica C **178**, 266 (1991).
[22]A. V. Boris, N. N. Kovaleva, O. V. Dolgov, T. Holden, C. T. Lin, B. Keimer, and C. Bernhard, Science **304**, 708 (2004).
[23]N. P. Armitage, R. Tediosi, F. Lévy, E. Giannini, L. Forro, and D. van der Marel, Phys. Rev. Lett. **104**, 237401 (2010).
[24]S. B. Nam, Phys. Rev. **156**, 487 (1967).
[25]O. V. Dolgov, R. K. Kremer, J. Kortus, A. A. Golubov, and S. V. Shulga, Phys. Rev. B **72**, 024504 (2005).
[26]A. A. Golubov and I. I. Mazin, Phys. Rev. B **55**, 15146 (1997).
[27]G. F. Chen, Z. Li, J. Dong, G. Li, W. Z. Hu, X. D. Zhang, X. H. Song, P. Zheng, N. L. Wang, and J. L. Luo, Phys. Rev. B **78**, 224512 (2008).
[28]M. Rotter, M. Tegel, and D. Johrendt, Phys. Rev. Lett. **101**, 107006 (2008).
[29]G. Mu, H. Luo, Z. Wang, L. Shan, C. Ren, and H.-H. Wen, Phys. Rev. B **79**, 174501 (2009).
[30]A. D. Christianson, E. A. Goremychkin, R. Osborn, S. Rosenkranz, M. D. Lumsden, C. D. Malliakas, I. S. Todorov, H. Claus, D. Y. Chung, M. G. Kanatzidis, R. I. Bewley, and T. Guidi, Nature (London) **456**, 930 (2008).
[31]The feedback of superconductivity on the spin-fluctuation spectrum observed by neutron scattering [30,37] was not considered in our model calculation.
[32]L. Boeri, O. V. Dolgov, and A. A. Golubov, Phys. Rev. Lett. **101**, 026403 (2008).
[33]By varying the effective coupling strength in our calculations, we found that this energy could be assigned to $\approx 4\Delta_A + \Omega$, where Ω is the peak frequency of the boson spectrum.
[34]See Supplemental Material at http:/link.aps.org/supplemental/10.1103/PhysRevB.84.174511 for interactive Java-based simulation.
[35]L. Fang, H. Luo, P. Cheng, Z. Wang, Y. Jia, G. Mu, B. Shen, I. I. Mazin, L. Shan, C. Ren, and H.-H. Wen, Phys. Rev. B **80**, 140508 (2009).
[36]A. I. Coldea, J. D. Fletcher, A. Carrington, J. G. Analytis, A. F. Bangura, J.-H. Chu, A. S. Erickson, I. R. Fisher, N. E. Hussey, and R. D. McDonald, Phys. Rev. Lett. **101**, 216402 (2008).
[37]D. S. Inosov, J. T. Park, P. Bourges, D. L. Sun, Y. Sidis, A. Schneidewind, K. Hradil, D. Haug, C. T. Lin, B. Keimer, and V. Hinkov, Nature Phys. **6**, 178 (2009).
[38]M. Tortello, D. Daghero, G. A. Ummarino, V. A. Stepanov, J. Jiang, J. D. Weiss, E. E. Hellstrom, and R. S. Gonnelli, Phys. Rev. Lett. **105**, 237002 (2010).
[39]F. Hardy, P. Burger, T. Wolf, R. A. Fisher, P. Schweiss, P. Adelmann, R. Heid, R. Fromknecht, R. Eder, D. Ernst, H. v. Löhneysen, and C. Meingast, Europhys. Lett. **91**, 47008 (2010).